Original Article

Feasibility of Ultrasonic Heating through Skull Phantom Using Single-element Transducer

Anastasia Antoniou, Christakis Damianou*

Department of Electrical Engineering, Computer Engineering and Informatics, Cyprus University of Technology, Limassol, Cyprus

Abstract

Background: Noninvasive neurosurgery has become possible through the use of transcranial focused ultrasound (FUS). This study assessed the heating ability of single element spherically focused transducers operating at 0.4 and 1.1 MHz through three-dimensional (3D) printed thermoplastic skull phantoms. **Methods:** Phantoms with precise skull bone geometry of a male patient were 3D printed using common thermoplastic materials following segmentation on a computed tomography head scan image. The brain tissue was mimicked by an agar-based gel phantom developed in-house. The selection of phantom materials was mainly based on transmission-through attenuation measurements. Phantom sonications were performed through water, and then, with the skull phantoms intervening the beam path. In each case, thermometry was performed at the focal spot using thermocouples. **Results:** The focal temperature change in the presence of the skull phantoms was reduced to less than 20 % of that recorded in free field when using the 0.4 MHz transducer, whereas the 1.1 MHz trans-skull sonication produced minimal or no change in focal temperature. The 0.4 MHz transducer showed better performance in trans-skull transmission but still not efficient. **Conclusion:** The inability of both tested single element transducers to steer the beam through the high attenuating skull phantoms and raise the temperature at the focus was confirmed, underlying the necessity to use a correction technique to compensate for energy losses, such those provided by phased arrays. The proposed phantom could be used as a cost-effective and ergonomic tool for trans-skull FUS preclinical studies.

Keywords: Agar phantom, heating, single element transducer, three-dimensional printed skull, trans-skull

Introduction

The last couple of decades, special research interest has been placed to the therapeutic value of ultrasound and the benefits it brings to many disciplines of modern medicine.[1,2] The noninvasive nature of focused ultrasound (FUS) constitutes its main advantage over conventional surgery. When operating at high intensities (in continuous mode), the mechanical energy is converted into heat inducing hyperthermic and ablative effects that so far were mainly exploited in the area of oncology for the ablative therapy of both shallow and deep tissue.[2] On the other hand, pulsed FUS is associated with various mechanical bioeffects from tissue vibrations to acoustic cavitation, which are caused by the fast pressure changes in tissue.[1]

In the 1950s, revolutionary studies were conducted by Fry *et al*.[3,4] to assess the high intensity focused ultrasound (HIFU) effects on the human brain tissue. However, transcranial focusing was unattainable because of the strong aberrating and attenuating nature of the skull resulting in significant beam defocusing.[5] Thereby, for many years, studies involved craniotomy for precise delivery of ultrasonic energy to the brain tissue through an acoustic window.[6]

In the 1990s, the multi-element ultrasonic technology has emerged as a way to actively form the beam compensating for such losses through regulating the phase of each element individually.[7,8] While this procedure was initially invasive, the introduction of numerical simulations for accurately estimating the resultant phase profile of the beam transmitted through the skull allowed for completely noninvasive transcranial applications.[9,10] In this regard, magnetic resonance imaging (MRI) was also a significant milestone that accelerated the adoption of this technology mainly through the

Received: 14-01-2023 **Revised:** 14-03-2023 **Accepted:** 31-03-2023 **Available Online:** 03-08-2023

Access this article online

Quick Response Code:

Website: https://journals.lww.com/jmut

DOI: 10.4103/jmu.jmu_3_23

Address for correspondence: Prof. Christakis Damianou, Department of Electrical Engineering, Computer Engineering and Informatics, Cyprus University of Technology, 30 Archbishop Kyprianou Street, Limassol 3036, Cyprus.
E-mail: christakis.damianou@cut.ac.cy

How to cite this article: Antoniou A, Damianou C. Feasibility of ultrasonic heating through skull phantom using single-element transducer. J Med Ultrasound 2024;32:32-40.

development of MR thermometry,[11] which is currently the only tool for monitoring temperature changes during sonication in almost real-time. Simultaneously, MRI is considered ideal as a guidance modality since it offers noninvasive optimal imaging of brain tumors without exposing patients to ionizing radiation.[12] Overall, these technological advances offered the accuracy required to safely target areas in the central nervous system without threatening adjacent or intervening tissues.

So far, the transcranial FUS technology has been investigated for its feasibility in treating essential tremor,[13] Parkinson's disease,[14] obsessive-compulsive disorder,[15] major depressive disorder,[15] and epilepsy.[16] The last years, a lot of research was devoted to investigating the use of this technology for tumor ablation and drug delivery by selective disruption of the blood − brain barrier (BBB).[17]

Currently, the available devices for brain ultrasound therapy in the clinic are limited. The SonoCloud (CarThera, France)[18] and NaviFUS (NaviFUS, Taiwan)[19] systems offer FUS plus microbubbles mediated disruption of the BBB. The first one comprises a nonfocused transducer that is implanted in the skull, whereas the later one offers neuronavigation-guided extracorporeal therapy. The ExAblate Neuro 4000 system (InSightec, Israel) is considered the leading magnetic resonance-guided FUS brain system and the first to be approved by the food and drug administration for targeted thermoablation of brain tissue.[20] Both extracorporeal systems use phased arrays for electronic steering of the beam.[19,20] The ExAblate system incorporates a helmet with 1024 elements operating at a frequency of 650 KHz, whereas the NaviFUS incorporates a more compact hemispherical transducer of fewer elements.

Although the phased array technology has immense benefits, it requires the use of sophisticated driving electronics that complicate its use and portability. Furthermore, it typically involves the use of a stereotactic frame making the procedure minimally invasive.[20] The high cost of this technology constitutes another shortcoming limiting its wider adaption, especially in the preclinical setting.

The use of a single-element transducer can could address these issues, but at the cost of difficulties in ultrasonic penetration through the skull. Successful trans-skull BBB disruption (BBBD) using a single element FUS transducer was achieved in experimental animals such as rabbits[21] and mice[22-25] by the administration of microbubble-enhanced pulsed FUS of 0.7 and 1.5 MHz, respectively. Single-element FUS transducers driven at a lower frequency of about 0.5 MHz were proven efficient for BBBD in larger animals, and particularly nonhuman primates.[26-31] Even lower frequencies of 0.4 and 0.25 MHz were chosen for similar applications in swine[32] and sheep,[33] respectively.

Simplified techniques for compensating for skull-induced energy losses were used in the effort to enable efficient trans-skull delivery of ultrasonic energy by single element transducers. As an example, a setup incorporating a single element 0.5 MHz spherical transducer for FUS-mediated BBBD was proposed by Marquet *et al*.[29] The proposed system is intended for use under stereotactic targeting and real-time monitoring by passive cavitation spectral analysis to enable MRI independent treatment sessions. In the framework of the system's evaluation, authors attempted BBBD of deep subcortical structures in macaque monkeys. The amplitude of ultrasonic emission was enhanced to compensate for the scalp and brain-induced attenuation losses as estimated by pressure measurements *in vitro*, thus leading to successful BBBD.

Pouliopoulos *et al*.[34] proposed a neuronavigation-guided system incorporating a single-element FUS transducer of 0.25 MHz nominal frequency, as well as a simulation framework for predicting the beam shift. The focusing properties of the transducer were assessed using a capsule hydrophone. The insertion of a human skull fragment in the beam path resulted in a pressure attenuation of about 45% compared to that measured in free field for a normal incidence angle, whereas a focal shift of 0.5 (±0.4) and 2.1 (±1.1) mm was observed along the lateral and axial dimensions, respectively.[34] Notably, the authors report a successful microbubbles-enhanced FUS-mediated BBB opening in the thalamus and dorsolateral prefrontal cortex of two nonhuman primates, which was evidenced by T1-weighted gadodiamide-enhanced MRI scans.[34] Notably, authors clarify that knowledge of the exact intracranial pressure with the proposed system is infeasible, and thus, the pressure field should be simulated utilizing computed tomography (CT) head scans of each subject individually.

More recently, the use of three-dimensional (3D) printed holographic acoustic lenses customized to each skull geometry have been proposed as a more comprehensive low-cost way to compensate for skull losses, thereby enabling transcranial therapy with a single-element transducer.[35,36] Maimbourg *et al*.[35] demonstrated a 10-fold increase in the accumulated energy in the targeted area using the specific approach of aberration correction with lenses.

This article provides insights on the use of single element FUS transducers with no other means of defocusing corrections for transcranial FUS in humans by preclinical experimentation using a brain-tissue/skull phantom setup. The optimal phantom to mimic brain tissue was selected among twelve agar-based phantoms prepared in house with different concentrations of agar, silicon dioxide, and evaporated milk. The selection was based on the ultrasonic attenuation property of these phantoms as estimated by the transmission-through technique. Rapid prototyping was used for the construction of a skull model. The ultrasonic attenuation in three common thermoplastic materials was initially assessed, from which two were deemed suitable to replicate the attenuation observed in the skull bone adequately. Therefore, two thermoplastic phantoms with the precise skull bone geometry of a male patient were 3D printed following segmentation on a CT head scan image.

The main part of the study involved HIFU sonications in the brain-tissue phantom through water (without any obstacle in

the beam's path), and then, with each skull phantom intervening the beam under the same experimental conditions. Single element spherically focused transducers of 0.4 and 1.1 MHz central frequency were used. In each case, thermometry during heating was performed at the focal spot using thermocouples.

Materials and Methods

No human participants or animals were included in the present study. Therefore, no informed consent or approval from an ethics committee was required.

Thermoplastic skull phantom

Development of block thermoplastic samples

Three solid blocks (100% infill) were 3D printed using the fused deposition modeling technique with acrylonitrile butadiene styrene (ABS, Stratasys) and VeroWhite Resin (RGD835, Stratasys) materials on a Stratasys printer (F270, Eden Prairie, Minnesota, USA), as well as with polylactic acid (PLA, 3DJ) thermoplastic on an ultimaker printer (3 Extended, Utrecht, Netherlands). The samples were modeled into flat plates of 5-mm thickness and 63 mm × 63 mm area, as shown in Figure 1.

Ultrasonic attenuation in thermoplastic samples

The ultrasonic attenuation in the thermoplastic samples was measured using a transmission-through immersion technique. Two identical transducers (custom-made, central frequency of 2.1 MHz and diameter of 10 mm) and the test-thermoplastic were fixed into a specially designed plastic holder ensuring the vertical incidence of the waves on the sample and minimizing energy losses due to refraction. The holder was submerged in degassed water and the first transducer was connected to the signal generator (33220A, Agilent, Santa Clara, CA 95051, United States), whereas the second transducer was connected to a digital oscilloscope (TDS 2012, Tektronix, Inc., 14150 SW Karl Braun Drive, United States) to display the received signal. The corresponding experimental setup is shown in Figure 2.

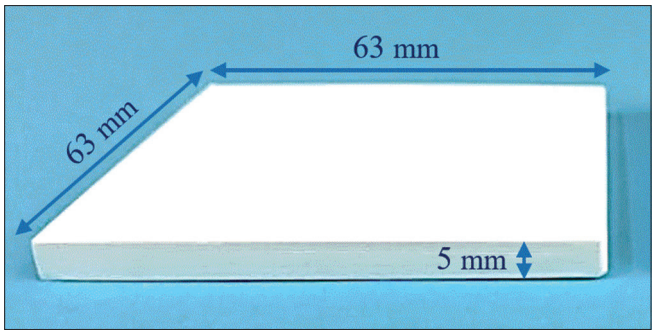

Figure 1: Photo of the 3D printed ABS flat plate with indicated dimensions. 3D: Three-dimensional, ABS: Acrylonitrile butadiene styrene

Pulsed ultrasound of 2.1 MHz frequency (20-cycle bursts with a period of 10 ms) was transmitted through the layered media. Initially, the peak-to-peak voltage was measured by the oscilloscope without any material between the transducers (reference signal). Then, the signal was recorded with the thermoplastic sample fixed in between the two transducers. The attenuation coefficient a of the sample was estimated by including the reference signal amplitude (A_w) and the one measured in the presence of the sample (A_s), together with the thickness of the sample x, and the transmission coefficient T of the water-sample interface in the following equation:[37]

$$a = a_w + \frac{20\,loge}{x} * \ln\left(\frac{A_w}{A_s}T\right) \quad (1)$$

in which α_w represents the attenuation coefficient of water. The transmission coefficient was estimated by the speed of sound in the samples using the widely known pulse-echo technique as previously described by Selfridge[38] All the measurements were conducted at room temperature (≅22°C).

Development of phantoms with skull geometry

The skull bone of an anonymized male patient was isolated following segmentation on CT head scan images. Figure 3a shows the stereolithography (STL) format of the whole human skull. For the purpose of this study, a circle-shaped part was isolated from the temporal region of the human skull model, and then imported in each printer's software in STL format for further processing. Samples were 3D printed in solid mode having a diameter of approximately 60 mm and a thickness

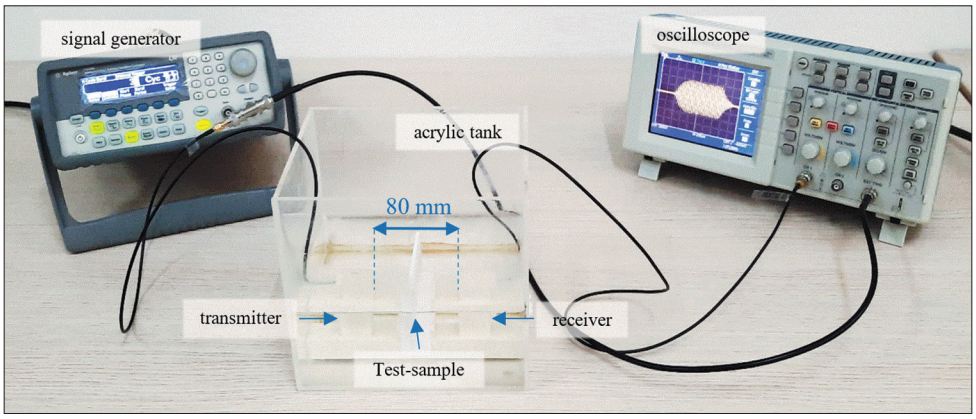

Figure 2: Photo of the experimental setup used to estimate the ultrasonic attenuation by the transmission-through method with indicated components

varying from 2.55 to 10.75 mm. The sample made with ABS (Stratasys) material is shown in Figure 3b.

Brain-tissue phantoms

Preparation of agar-based phantoms

Phantoms were prepared according to the procedure previously described by Drakos *et al*.[39] using agar (Merck KGaA, EMD Millipore Corporation, Darmstadt, Germany) as the gelling agent while silicon dioxide (Sigma-Aldrich, St. Louis, Missouri, United States) and evaporated milk (Nounou, Friesland Campina, Marousi, Greece) were included as modifiers of ultrasonic scattering and absorption, respectively.[40] Agar-only samples were prepared with different agar concentration of 2%, 4%, 6%, and 8% weight per volume (w/v). Silica-doped phantoms were prepared using a silicon dioxide powder concentration of 2%, 4%, 6%, 8%, and 10% w/v for a constant agar concentration of 6% w/v. The effect of evaporated milk concentration was assessed by including different volume per volume (v/v) concentrations of 10%, 20%, and 30% (replacing a percentage of the water component) at solutions with fixed concentrations of 6% w/v agar and 4% w/v silicon dioxide. For each recipe, the solution was poured in two molds of different thickness (20 and 40 mm) and left to solidify to form the final phantoms, as shown in the photo of Figure 4.

Ultrasonic attenuation in agar-based gels

The ultrasonic attenuation coefficient of the developed agar-based phantoms was estimated (at 22°C) using the previously presented experimental set-up [Figure 2] but a quite different procedure known as the variable thickness method[41] to assess which one matches better the acoustic characteristics of the brain tissue. The specific method involves the comparison of ultrasonic signals acquired through the samples of different thickness for estimating the attenuation coefficient (in units of dB/cm) through the following formula:[41]

$$a = \frac{20}{X_2 - X_1} * log\left(\frac{A_{x2}}{A_{x1}}\right) \quad (2)$$

Where A_{x1} and A_{x2} symbolize the peak-to-peak voltages in the presence of the thinner ($\chi = 20$ mm) and thicker ($\chi^2 = 40$ mm) samples [Figure 4], respectively.

Thermometry during high-intensity focused ultrasound in brain tissue/skull phantom

The property of the skull phantoms to obstruct the propagation of acoustic waves generated by a single element transducer was evaluated by sonicating the agar-based phantom that was deemed suitable to mimic brain tissue (6% w/v agar and 4% w/v silicon dioxide). For proper HIFU exposures, a special holder was 3D printed to accommodate the focused transducer and the phantom in a water tank, thus ensuring a normal incidence angle. Specifically, the transducer was fixed at the bottom part facing toward the phantom, as shown in Figure 5. The holder was geometrically designed to allow horizontal insertion of a thermocouple in the phantom every 5 mm. Therefore, the focal spot was easily located enabling recording of the temperature

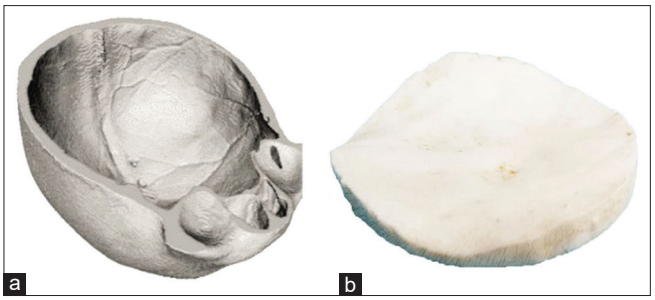

Figure 3: (a) STL format of the whole skull model. (b) 3D printed skull phantom. 3D: Three-dimensional. STL: Stereolithography

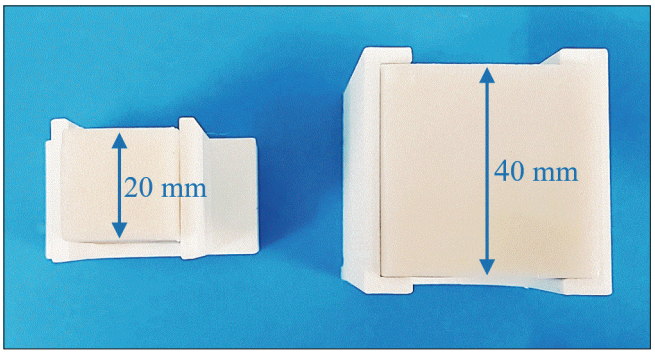

Figure 4: Top view of the thinner and thicker agar-based phantoms

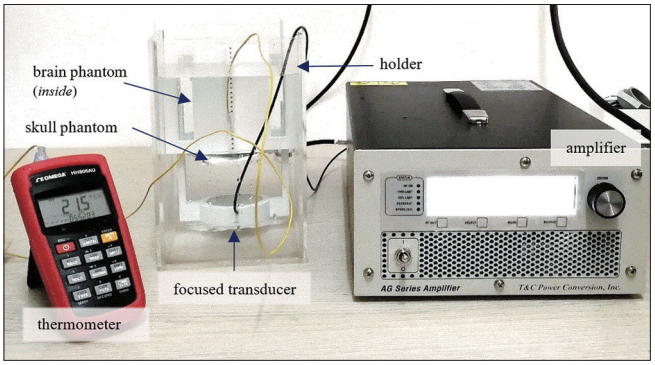

Figure 5: Photo of the experimental setup used to estimate temperature changes in the phantom during heating, showing the designed holder and the location of the compartments

changes using a thermometer (Omega Thermometer, HH806AU, Omega Engineering, USA). As illustrated in Figure 5, the holder also included a special structure underneath the phantom's location to accommodate the skull sample. Degassed water was poured inside the tank until it reached the top level of the phantom serving as the coupling medium.

The transducer was connected to an amplifier (AG1012, AG Series Amplifier, T and G Power Conversion, Inc.) with a build-in signal generator. Sonications were performed with two different single element spherically focused transducers (Sonic concepts, Washington, USA). The first one had a central frequency of 1.1 MHz, radius of curvature of 100 mm, and diameter of 40 mm, whereas the second one had a central frequency of 0.4 MHz, radius of curvature of 70 mm, and

diameter of 40 mm. The acoustic efficacy of both transducers was approximately 100%. The distance between the bottom of the phantom and each transducer was properly adjusted so that the focal depth is 2.5 cm for both. Temperature measurements were acquired using a thermometer (HH806AU, Omega Engineering, USA) with a sampling rate of 1s. First, the temperature evolution during sonication was recorded through water path (without any plastic phantom), and then, in the presence of each skull phantom sequentially. For the sake of comparison, the experiment was also conducted with a 3-mm ABS flat plate inserted in the pathway of the beam.

Results

Ultrasonic attenuation in thermoplastic samples

The attenuation of ultrasonic waves in the 3D printed thermoplastic samples (5-mm thick solid plates) was estimated using a common transmission-through technique and pulsed ultrasound of 2.1 MHz frequency. The mean attenuation coefficient was estimated at 8.4 ± 0.2 dB/cm for the Resin (Stratasys), at 14.9 ± 0.6 dB/cm for the PLA (3DJ) and at 37.7 ± 1.8 dB/cm for the ABS (Stratasys). The estimated coefficient of the resin material was considered small compared to the values reported literally for the skull bone.[5,42,43] Therefore, the PLA and ABS thermoplastics were used for the construction of phantoms with precise geometry of a human skull, thus more accurately replicating the distortion and attenuation effects of the skull.

Ultrasonic attenuation in agar-based gels

Twelve agar-based phantoms were developed with varying concentrations of agar, silicon dioxide, and evaporated milk. The results suggest that the attenuation of ultrasonic waves is enhanced with increasing concentration of each inclusion (agar, silicone dioxide, and evaporated milk). Figure 6 shows the trend for the gels containing only agar. The corresponding results for the silica- and evaporated milk-doped phantoms are shown in Figures 7 and 8, respectively.

The phantom containing 6% w/v agar and 4% w/v silicon dioxide was found to possess an attenuation coefficient (0.75 ± 0.06 dB/cm-MHz) in the range of 0.65–0.95 dB/cm-MHz reported literally for brain tissues[44] and deemed suitable to mimic brain tissue in subsequent experiments.

Thermometry during high-intensity focused ultrasound in brain-tissue/skull phantom

These experiments aimed to assess the feasibility of two single element transducers of different frequency to heat up the soft-tissue phantom through the skull mimics by performing high power sonications. The selected phantom containing 6% agar and 4% silicon dioxide served as the brain tissue mimic.

The thermometry data obtained by thermocouple measurements are listed in Table 1, including the transducer characteristics and the corresponding temperature changes achieved at the focal depth of 2.5 cm in free field (through water), as well as in the presence of each skull phantom. Figures 9 and 10 show

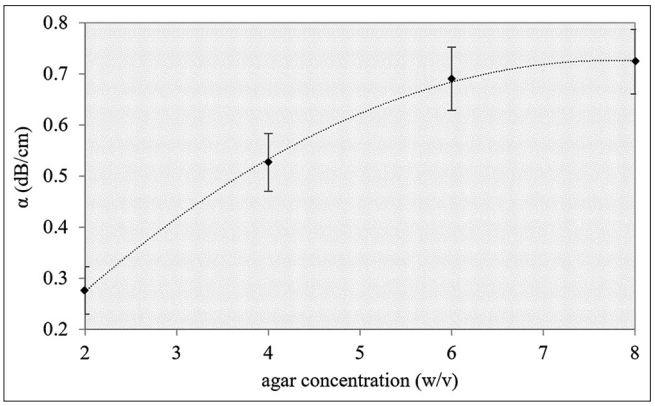

Figure 6: The mean attenuation coefficient (at 1.1 MHz) plotted against the agar concentration. The data points were fitted by polynomial regression. The error bars correspond to the standard deviation

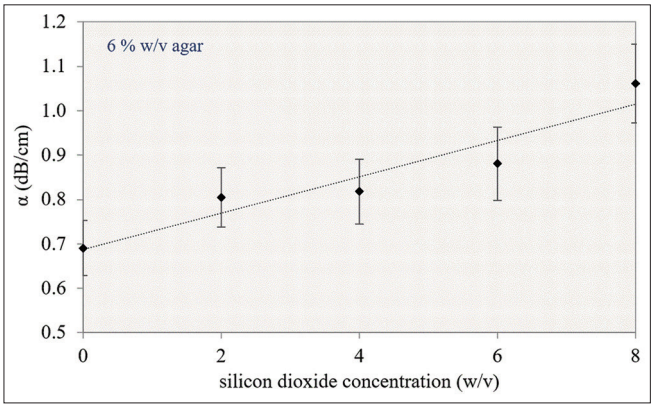

Figure 7: The mean attenuation coefficient (at 1.1 MHz) plotted against the silicon dioxide concentration for a fixed amount of 6% w/v agar. The data points were fitted by linear regression. The error bars correspond to the standard deviation

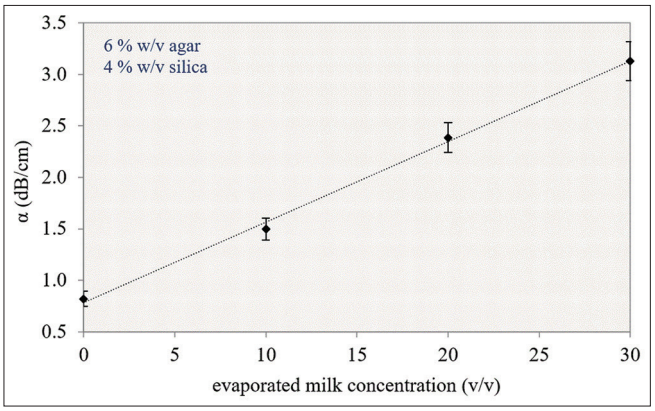

Figure 8: The mean attenuation coefficient (at 1.1 MHz) plotted against the evaporated milk concentration for a fixed amount of 6% w/v agar and 4% w/v silicon dioxide. The data points were fitted by linear regression. The error bars correspond to the standard deviation

the corresponding temperature profiles (temperature change versus time) recorded in the phantom using the 0.40 MHz (diameter of 40 mm and radius of curvature of 70 mm) and 1.10 MHz (diameter of 50 mm and radius of curvature of

Table 1: List of transducer specifications, including operating frequency, diameter and radius of curvature and the corresponding temperature changes recorded using acoustical power of 30 W for 30 s at the focal depth of 2.5 cm with no plastic, as well as with the acrylonitrile butadiene styrene and polylactic acid phantoms intervening the beam path

Transducer characteristics			Thermometry results ΔT (°C)			
Frequency (MHz)	Diameter (mm)	Radius of curvature (mm)	No skull	PLA skull (α≅15 dB/cm)	ABS skull (α≅38 dB/cm)	ABS flat sample (3 mm)
0.4	40	70	15.7	1.9	2.7	-
1.1	40	100	24.7	0	0.4	2.2

PLA: Polylactic acid, ABS: Acrylonitrile butadiene styrene

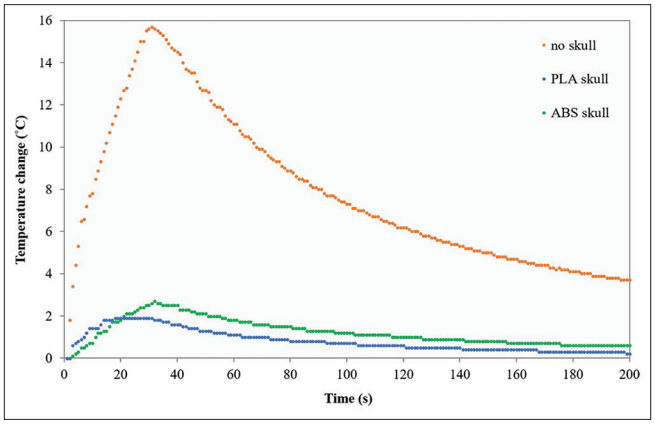

Figure 9: Temperature change versus time recorded in agar-based phantom at focal depth of 2.5 cm during sonication at acoustic power of 30 W for 30 s using the 0.4 MHz transducer (diameter = 40 mm and radius of curvature = 70 mm) with no skull, as well as with the skull phantoms inserted in the beam path

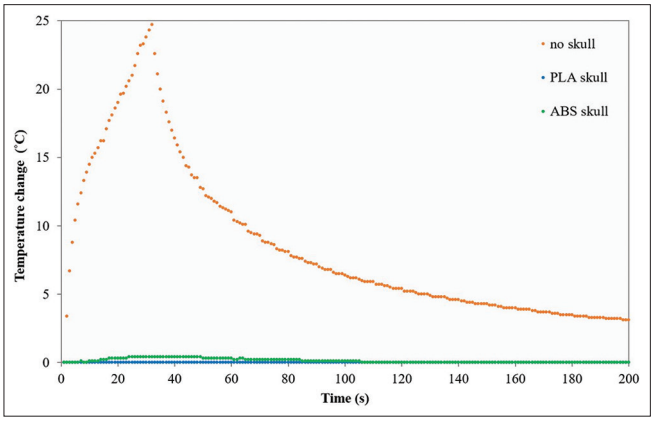

Figure 10: Temperature change versus time recorded in agar-based phantom at focal depth of 2.5 cm during sonication at acoustical power of 30 W for 30 s using the 1.1 MHz transducer (diameter = 40 mm and radius of curvature = 100 mm) with no skull, as well as with the skull phantoms inserted in the beam path

100 mm) transducers, respectively. During sonication, heat absorption was responsible for the temperature rise while conduction decreased the rate of temperature elevation, whereas postsonication only conduction mechanism remained, thus resulting in temperature reduction. As expected, the temperature change at the focal point is significantly reduced when the ultrasonic waves are obstructed by the skull phantoms.

Discussion

This study aimed to examine the performance of single element spherically focused transducers in terms of trans-skull heating of tissue. Phantoms constitute a cost-effective and ergonomic tool for evaluating the performance of ultrasonic equipment.[40] In this study, an agar-based phantom was prepared to mimic brain tissue, whereas the skull was mimicked by a 3D printed thermoplastic skull model. The selection of agar as the gelling agent was based on that agar gels were proven very promising for the use with the FUS technology, as well as on their cost-effectiveness and ease of preparation.[40]

The 3D printing technology is continuously gaining popularity as a cost-effective tool for rapid prototyping, offering the ability to design structures of complex geometry with high precision.[45,46] In the last decade, it has been increasingly employed for the construction of bone mimicking phantoms using thermoplastic materials,[45,47-49] including MRI compatible skull phantoms embedding tissue-mimicking gels or freshly excised tissue.[47,49] Skull phantoms were initially manufactured with a simplified geometry[47] and later with the precise geometry of a real human skull as extracted from brain CT scans.[49] More recently, a 3D printed skull filled with a phantom mimicking both the vessels and tissue in the cranium has been proposed.[50] These phantoms were designed to match the ultrasonic properties of human skull. Accordingly, in this study, two anthropomorphic skull models were 3D printed using two different thermoplastic materials, which were selected based on transmission-through ultrasonic attenuation measurements.

The longitudinal attenuation coefficient of three common 3D printing thermoplastics was estimated using a transmission-through technique. The estimated attenuation coefficient of the Resin sample (8.4 ± 0.2 dB/cm) was considered small compared to the literature values for skull bone. Ammi *et al*.[43] report attenuation values in the temporal bone of 13.4–22.14 dB/cm at 1 MHz and 34.2–48.5 dB/cm at 2 MHz for skulls not presenting temporal bone window insufficiency. Therefore, the PLA and ABS samples with mean attenuation coefficients of 14.9 (±0.6) and 37.7 (±1.8) dB/cm were deemed more suitable to replicate the insertion energy loss in human skull bone and used for skull phantom development. Note that the high ultrasonic attenuation reported

for the skull bone is related to the varying thickness, porosity of the cancellous bone and other inhomogeneities, which serve as additional sources of attenuation not existing in thermoplastic samples.

Phantoms were then prepared following accurate geometrical replication of a human skull to account for the defocusing effects induced by the varying thickness of the skull. The skull bone geometry of a male adult was obtained from CT head scans and a circle shape part was isolated from the temporal region, which constitutes an optimal window for transcranial delivery of ultrasonic energy.[43] Phantoms were 3D printed in solid mode using the selected thermoplastic materials (ABS, Stratasys and PLA, 3DJ).

The approach utilized in this study suffers from the limitation that the candidate thermoplastic materials were only investigated in terms of ultrasonic attenuation. However, thermoplastics were previously proven capable of sufficiently matching the propagation velocity of ultrasonic waves in the human skull as well.[37,50] Of course, given that in the real scenario ultrasonic waves interact with the complex microstructure of the bone (i.e., multilayer structure including cancellous bone), the proposed phantom constitutes a much simplified model of the human skull. However, since it was 3D printed with the exact geometry of a human skull, beam aberration mechanisms due to the varying skull thickness can be considered consistent between the phantom and real human skull. Overall, the phantom was considered sufficiently realistic for the purpose of the current study.

Gel phantoms were prepared with varying concentrations of agar, silicone dioxide, and evaporated milk to achieve different levels of ultrasonic attenuation. The attenuation results estimated by the variable thickness methodology suggest that attenuation increases with increasing w/v concentration of agar from 2% to 8% [Figure 6] following a second order polynomial ($R^2 = 0.99$). The influence of the evaporated milk concentration on the resultant attenuation followed a linear pattern ($R^2 = 0.99$). Increasing silicon dioxide concentration also enhanced attenuation, though not in a specific trend [Figure 7]. In line with our findings, a positive linear relation between attenuation and concentration of milk was previously reported in the literature.[49] Notably, the role of these inclusions was examined in previous studies, in which silica particles were found to enhance acoustic scattering,[51] whereas evaporated milk was proven a key absorber of ultrasonic energy.[40]

Phantoms doped with silicon dioxide at concentrations of 2, 4, and 6% w/v (6% w/v agar) were found to possess attenuation coefficient values that fall well in the range of 0.65-0.95 dB/cm-MHz reported literally for brain tissues.[44] However, solutions with silica concentrations of more than 4% undergo rapid solidification and are more likely to contain inhomogeneities. Therefore, the phantoms doped with 2%–4% w/v silicon dioxide were deemed suitable to mimic brain tissue. Since almost equal attenuation coefficient was estimated for both recipes, the one with 4% w/v silica was selected to be used in subsequent experiments. Moreover, agar/silica phantoms are more stable and durable than milk-doped phantoms.

The heating properties of two single element transducers through the developed skull phantoms were investigated by thermocouple measurements in the brain tissue phantom (6% w/v agar and 4% w/v silica). The phantoms were mounted on a specially designed set-up being immersed in degassed water for proper ultrasonic propagation. Thermal profiles at the focus (2.5 cm) were recorded during sonications at acoustic power of 30 W. Absorption was the responsible mechanism for temperature rise in the agar gel, whereas upon deactivation of the transducer conduction-induced heat loss occurred. It is interesting that in the presence of the skull phantoms the thermal profiles presented plateaus where the temperature remained constant for several seconds revealing that the rate of heat deposition was very slow.

Without any sample along the beam's path, the 1.1 MHz sonication caused bigger temperature change (24.7°C) compared to the 0.4 MHz sonication (15.7°C) despite the use of similar acoustic parameters (acoustical power 30 W for 30 s). This is attributed to the fact that the 0.4 MHz beam is wider, and thereby, the produced intensities are lower. In fact, the focusing capability is determined by the transducer characteristics; frequency (f), radius of curvature (R), and diameter (D). Alternatively, when the focal depth and diameter are combined into the *f*-number (=*R/D*), the focus effect is determined by the *f*-number and frequency. For single element spherically focused transducers the focal beam diameter (cross section) equals to λ* f-number (where λ is the wavelength), thus being proportional to the *f*-number and inversely proportional to frequency. For the tested 1.1 and 0.4 MHz transducers, the beam radius at the focal depth equals to about 0.17 cm and 0.33 cm, respectively. Accordingly, the applied acoustic power of 30 W corresponds to focal intensities of 329 W/cm^2 and 89 W/cm^2 for the 1.1 and 0.4 MHz transducers. Therefore, without the skull mimic, the 1.1 MHz transducer results in higher temperature increase at the focus.

Nevertheless, in the presence of the skull phantoms a larger temperature change was recorded using the 0.4 MHz focused transducer. It seems that the phenomenon of scattering is the major factor responsible for this observation. Even though the 0.4 MHz transducer produces a wider beam, it seems that a larger amount of ultrasonic energy propagates through the thermoplastic samples due to the decreased scattering occurring at lower frequencies. Overall, the 0.4 MHz transducer showed better performance in trans-skull transmission. Notably, the use of such low frequencies is widely reported in studies involving nonhuman primates and large animals[26-33] and is driven by the highly aberrating nature of the skull bone. It should be though noted that these studies exploit the mechanical rather than the thermal effects of FUS.

The propagation of ultrasonic waves by single element emissions was blocked to a great degree by the skull phantoms,

leading to minimal temperature increase at the focal point. In fact, the focal temperature change in the presence of the skull phantoms was reduced to less than 20% of that recorded in free filed. This is attributed to the high ultrasonic attenuation occurring in the phantoms, but also to the defocusing effects of the varying thickness that were proven to cause spreading of the beam and focal shift.[34] Notably, the strong defocusing effects of an ABS skull model were previously demonstrated using MR thermometry in a gel phantom[49] and were associated with a great temperature reduction at the focal region.[49] This is where the phased array approach takes effect.

The specific mechanisms of energy loss through the skull phantoms such as the aforementioned beam defocusing were not explored quantitatively in the current study and may be addressed in a future study. Qualitative assessment was though performed by comparing the temperature evolution during sonication at 1.1 MHz through the ABS skull phantom with that recorded for a flat sample using similar acoustic parameters. With the skull phantom intervening the beam path, a minimal temperature change of 0.4°C was achieved. The flat sample resulted in the bigger temperature rise of 2.2°C, confirming that the thickness variability of the skull phantom induced greater energy losses.

Single element transducers were proven efficient for transcranial applications in small experimental animals such as mice[22-25] because of their thin skull bone. Furthermore, many studies report the successful use of this technology for BBBD in nonhuman primates,[26-31] whose skull resembles better the human skull. It should be though noted that these applications exploit the mechanical-cavitational effects of FUS rather than the thermal effects. Even in that case, there are many safety concerns, and thus, precise refocusing techniques are needed to compensate for energy losses and focal shifts, thus achieving accurate targeting and sufficient deposition of energy without threatening sensitive brain structures.

Overall, the herein findings confirm the inability of a single element transducer to efficiently steer the beam through the human skull to impart thermal effects to tissue unless a comprehensive correction technique is applied. The phased array technology is still considered the only tool offering optimal deposition of ultrasonic energy in the brain while maintaining the safety levels required in the clinical setting. Recently, the use of 3D printed lenses to compensate beam aberrations while using single-element transducers has been proposed;[35,36] however, further investigation is required to verify these findings and prove the feasibility of this approach. The proposed brain tissue-skull phantom could constitute a useful cost-effective tool for preclinical studies in the field of transcranial FUS.

Financial support and sponsorship

The study was co-funded by the European Structural and Investment Funds (ESIF) and the Republic of Cyprus through the Research and Innovation Foundation (RIF) under the project SOUNDPET (INTEGRATED/0918/0008).

Conflicts of interest

There are no conflicts of interest.

References

1. Izadifar Z, Izadifar Z, Chapman D, Babyn P. An introduction to high intensity focused ultrasound: Systematic review on principles, devices, and clinical applications. J Clin Med 2020;9:460.
2. Duc NM, Keserci B. Emerging clinical applications of high-intensity focused ultrasound. Diagn Interv Radiol 2019;25:398-409.
3. Fry WJ, Mosberg WH Jr., Barnard JW, Fry FJ. Production of focal destructive lesions in the central nervous system with ultrasound. J Neurosurg 1954;11:471-8.
4. Barnard JW, Fry WJ, Fry FJ, Krumins RF. Effects of high intensity ultrasound on the central nervous system of the cat. J Comp Neurol 1955;103:459-84.
5. Fry FJ, Barger JE. Acoustical properties of the human skull. J Acoust Soc Am 1978;63:1576-90.
6. Guthkelch AN, Carter LP, Cassady JR, Hynynen KH, Iacono RP, Johnson PC, *et al.* Treatment of malignant brain tumors with focused ultrasound hyperthermia and radiation: Results of a phase I trial. J Neurooncol 1991;10:271-84.
7. Tanter M, Thomas JL, Fink M. Focusing and steering through absorbing and aberrating layers: Application to ultrasonic propagation through the skull. J Acoust Soc Am 1998;103:2403-10.
8. Hynynen K, Jolesz FA. Demonstration of potential noninvasive ultrasound brain therapy through an intact skull. Ultrasound Med Biol 1998;24:275-83.
9. Sun J, Hynynen K. Focusing of therapeutic ultrasound through a human skull: A numerical study. J Acoust Soc Am 1998;104:1705-15.
10. Aubry JF, Tanter M, Pernot M, Thomas JL, Fink M. Experimental demonstration of noninvasive transskull adaptive focusing based on prior computed tomography scans. J Acoust Soc Am 2003;113:84-93.
11. Rieke V, Butts Pauly K. MR thermometry. J Magn Reson Imaging 2008;27:376-90.
12. González Hernando C, Esteban L, Cañas T, Van den Brule E, Pastrana M. The role of magnetic resonance imaging in oncology. Clin Transl Oncol 2010;12:606-13.
13. Health Quality Ontario. Magnetic resonance-guided focused ultrasound neurosurgery for essential tremor: A health technology assessment. Ont Health Technol Assess Ser 2018;18:1-141.
14. Foffani G, Trigo-Damas I, Pineda-Pardo JA, Blesa J, Rodríguez-Rojas R, Martínez-Fernández R, *et al.* Focused ultrasound in Parkinson's disease: A twofold path toward disease modification. Mov Disord 2019;34:1262-73.
15. Chang KW, Jung HH, Chang JW. Magnetic resonance-guided focused ultrasound surgery for obsessive-compulsive disorders: Potential for use as a novel ablative surgical technique. Front Psychiatry 2021;12:640832.
16. Abe K, Yamaguchi T, Hori H, Sumi M, Horisawa S, Taira T, *et al.* Magnetic resonance-guided focused ultrasound for mesial temporal lobe epilepsy: A case report. BMC Neurol 2020;20:160.
17. Lee EJ, Fomenko A, Lozano AM. Magnetic resonance-guided focused ultrasound: Current status and future perspectives in thermal ablation and blood-brain barrier opening. J Korean Neurosurg Soc 2019;62:10-26.
18. Idbaih A, Canney M, Belin L, Desseaux C, Vignot A, Bouchoux G, *et al.* Safety and feasibility of repeated and transient blood-brain barrier disruption by pulsed ultrasound in patients with recurrent glioblastoma. Clin Cancer Res 2019;25:3793-801.
19. Chen KT, Lin YJ, Chai WY, Lin CJ, Chen PY, Huang CY, *et al.* Neuronavigation-guided focused ultrasound (NaviFUS) for transcranial blood-brain barrier opening in recurrent glioblastoma patients: Clinical trial protocol. Ann Transl Med 2020;8:673.
20. Meng Y, Jones RM, Davidson B, Huang Y, Pople CB, Surendrakumar S, *et al.* Technical principles and clinical workflow of transcranial MR-guided focused ultrasound. Stereotact Funct Neurosurg 2021;99:329-42.
21. Hynynen K, McDannold N, Sheikov NA, Jolesz FA, Vykhodtseva N. Local and reversible blood-brain barrier disruption by noninvasive focused ultrasound at frequencies suitable for trans-skull sonications.

Neuroimage 2005;24:12-20.
22. Choi JJ, Pernot M, Small SA, Konofagou EE. Noninvasive, transcranial and localized opening of the blood-brain barrier using focused ultrasound in mice. Ultrasound Med Biol 2007;33:95-104.
23. Choi JJ, Wang S, Tung YS, Morrison B 3rd, Konofagou EE. Molecules of various pharmacologically-relevant sizes can cross the ultrasound-induced blood-brain barrier opening *in vivo*. Ultrasound Med Biol 2010;36:58-67.
24. Choi JJ, Selert K, Gao Z, Samiotaki G, Baseri B, Konofagou EE. Noninvasive and localized blood-brain barrier disruption using focused ultrasound can be achieved at short pulse lengths and low pulse repetition frequencies. J Cereb Blood Flow Metab 2011;31:725-37.
25. Wang S, Samiotaki G, Olumolade O, Feshitan JA, Konofagou EE. Microbubble type and distribution dependence of focused ultrasound-induced blood-brain barrier opening. Ultrasound Med Biol 2014;40:130-7.
26. Wu SY, Tung YS, Marquet F, Downs M, Sanchez C, Chen C, *et al.* Transcranial cavitation detection in primates during blood-brain barrier opening – A performance assessment study. IEEE Trans Ultrason Ferroelectr Freq Control 2014;61:966-78.
27. Samiotaki G, Karakatsani ME, Buch A, Papadopoulos S, Wu SY, Jambawalikar S, *et al.* Pharmacokinetic analysis and drug delivery efficiency of the focused ultrasound-induced blood-brain barrier opening in non-human primates. Magn Reson Imaging 2017;37:273-81.
28. Wu SY, Aurup C, Sanchez CS, Grondin J, Zheng W, Kamimura H, *et al.* Efficient blood-brain barrier opening in primates with neuronavigation-guided ultrasound and real-time acoustic mapping. Sci Rep 2018;8:7978.
29. Marquet F, Teichert T, Wu SY, Tung YS, Downs M, Wang S, *et al.* Real-time, transcranial monitoring of safe blood-brain barrier opening in non-human primates. PLoS One 2014;9:e84310.
30. Marquet F, Tung YS, Teichert T, Ferrera VP, Konofagou EE. Noninvasive, transient and selective blood-brain barrier opening in non-human primates *in vivo*. PLoS One 2011;6:e22598.
31. Karakatsani ME, Samiotaki GM, Downs ME, Ferrera VP, Konofagou EE. Targeting effects on the volume of the focused ultrasound-induced blood-brain barrier opening in nonhuman primates *in vivo*. IEEE Trans Ultrason Ferroelectr Freq Control 2017;64:798-810.
32. Wei KC, Tsai HC, Lu YJ, Yang HW, Hua MY, Wu MF, *et al.* Neuronavigation-guided focused ultrasound-induced blood-brain barrier opening: A preliminary study in swine. AJNR Am J Neuroradiol 2013;34:115-20.
33. Yoon K, Lee W, Chen E, Lee JE, Croce P, Cammalleri A, *et al.* Localized blood-brain barrier opening in ovine model using image-guided transcranial focused ultrasound. Ultrasound Med Biol 2019;45:2391-404.
34. Pouliopoulos AN, Wu SY, Burgess MT, Karakatsani ME, Kamimura HA, Konofagou EE. A clinical system for non-invasive blood-brain barrier opening using a neuronavigation-guided single-element focused ultrasound transducer. Ultrasound Med Biol 2020;46:73-89.
35. Maimbourg G, Houdouin A, Deffieux T, Tanter M, Aubry JF. 3D-printed adaptive acoustic lens as a disruptive technology for transcranial ultrasound therapy using single-element transducers. Phys Med Biol 2018;63:025026.
36. Ferri M, Bravo JM, Redondo J, Sánchez-Pérez JV. Enhanced numerical method for the design of 3-D-printed holographic acoustic lenses for aberration correction of single-element transcranial focused ultrasound. Ultrasound Med Biol 2019;45:867-84.
37. Antoniou A, Evripidou N, Giannakou M, Constantinides G, Damianou C. Acoustical properties of 3D printed thermoplastics. J Acoust Soc Am 2021;149:2854.
38. Selfridge AR. Approximate material properties in isotropic materials. IEEE Trans Sonics Ultrason 1985;SU-32:381-3.
39. Drakos T, Giannakou M, Menikou G, Constantinides G, Damianou C. Characterization of a soft tissue-mimicking agar/wood powder material for MRgFUS applications. Ultrasonics 2021;113:106357.
40. Antoniou A, Damianou C. MR relaxation properties of tissue-mimicking phantoms. Ultrasonics 2022;119:106600.
41. Menikou G, Damianou C. Acoustic and thermal characterization of agar based phantoms used for evaluating focused ultrasound exposures. J Ther Ultrasound 2017;5:14.
42. Pichardo S, Sin VW, Hynynen K. Multi-frequency characterization of the speed of sound and attenuation coefficient for longitudinal transmission of freshly excised human skulls. Phys Med Biol 2011;56:219-50.
43. Ammi AY, Mast TD, Huang IH, Abruzzo TA, Coussios CC, Shaw GJ, *et al.* Characterization of ultrasound propagation through *ex-vivo* human temporal bone. Ultrasound Med Biol 2008;34:1578-89.
44. Selbekk T, Jakola AS, Solheim O, Johansen TF, Lindseth F, Reinertsen I, *et al.* Ultrasound imaging in neurosurgery: Approaches to minimize surgically induced image artefacts for improved resection control. Acta Neurochir (Wien) 2013;155:973-80.
45. Menikou G, Yiannakou M, Yiallouras C, Ioannides C, Damianou C. MRI-compatible breast/rib phantom for evaluating ultrasonic thermal exposures. Int J Med Robot 2018;14. DOI: 10.1002/rcs.1849.
46. Shen Z, Yao Y, Xie Y, Guo C, Shang X, Dong X, *et al.* The process of 3D printed skull models for anatomy education. Comput Assist Surg (Abingdon) 2019;24:121-30.
47. Hadjisavvas V, Mylonas N, Ioannides K, Damianou C. An MR-compatible phantom for evaluating the propagation of high intensity focused ultrasound through the skull. AIP Conf Proc 2012;1481:119-24.
48. Menikou G, Yiannakou M, Yiallouras C, Ioannides C, Damianou C. MRI-compatible bone phantom for evaluating ultrasonic thermal exposures. Ultrasonics 2016;71:12-9.
49. Menikou G, Dadakova T, Pavlina M, Bock M, Damianou C. MRI compatible head phantom for ultrasound surgery. Ultrasonics 2015;57:144-52.
50. Bai C, Ji M, Bouakaz A, Zong Y, Wan M. Design and characterization of an acoustically and structurally matched 3-D-printed model for transcranial ultrasound imaging. IEEE Trans Ultrason Ferroelectr Freq Control 2018;65:741-8.
51. Partanen A, Mougenot C, Vaara T. Feasibility of agar-silica phantoms in quality assurance of MRgHIFU. AIP Conf Proc 2009;1113:296-300.